# Study of hardness distribution in a rail welded joint after welding with accelerated cooling

***A. I. Karlina**, Cand. Eng., Scientific Researcher* [1], *e-mail: karlinat@mail.ru;*
***V. V. Kondratyev,** Cand. Eng., Senior Scientific Researcher* [2];
***V. E. Gozbenko,** Dr. Eng., Prof.* [3, 4];
***R. V. Kononenko,** Cand. Eng.* [5]

[1] *Moscow State University of Civil Engineering (Moscow, Russia);*
[2] *A. P. Vinogradov Institute of Geochemistry of the Siberian Branch of the Russian Academy of Sciences (Irkutsk, Russia);*
[3] *Irkutsk State Transport University (Irkutsk, Russia);*
[4] *Angarsk State Technical University (Angarsk, Russia);*
[5] *Irkutsk National Research Technical University (Irkutsk, Russia)*

In order to improve parameters of rails and railroad wheels, it is necessary to examine new microstructures, new technologies for production and processing of rails. Pearlitic steels are widely used in the railroad industry worldwide, due to their good wear resistance and satisfactory impact strength, as well as due to their relatively low production cost. Mechanical properties of pearlitic steels are controlled by microstructure, which is created as a result of thermomechanical treatment, especially by such parameters as austenite grain size, interlamellar spacing in pearlite and dimension of a pearlite colony. Essential microstructural variations occur along the heat-affected area in the process of butt welding of rails. Significant variations of hardness and other mechanical properties in a metal welded joint are connected with cementite morphology. A soft area, which is observed in the heat-affected area of a welded joint and which is caused by cementite spheroidizing, leads to local hardness loss. The experimental results on evaluation of cooling rate influence in a rail welded joint on hardness in the heat-affected area are presented in this research. It was confirmed that variation of cooling rate influence in a rail welded joint finalizes in variation of spheroidizing tendency in the areas of lowered hardness.

***Key words:*** pearlite, ferrite, cementite, welding, butt welding, melting, rails, impact strength, cooling rate, wear, hardness.
***DOI:*** 10.17580/cisisr.2024.02.10

## Introduction

Pearlite steels are widely used in the railroad industry. Standard pearlite rails, which are characterized by relatively simple eutectoid chemical composition, have relatively large interlamellar spacing and thereby relatively low hardness values (about 300 HB). Premium class rails with optimized chemical composition are characterized by more fine pearlitic microstructure and, respectively, higher hardness within the range 340–390 HB [1–5]. However, despite the real technical knowledge on pearlitic rail steels, which are used worldwide at present time, many authors noted periodical cases of premature rejects, leading to large financial losses and sometimes to human losses [6, 7]. Most part of these rejects are connected with war, fatigue and welding problems. The conventional method of rails connection is concluded in their bolt joining, but railroad goes out of service owing to dynamic loads, while technical maintenance expenses are very high. In order to minimize this problem, the rail welding technology was developed, which displayed evident improvements [8–13]. There are two main types of rail welding processes: (1) flash butt welding (FBW) and (2) termite (aluminothermic) welding. Use of continuously welded rails with FBW constitutes approximately 80 % of welded seams for rails worldwide due to their better quality [6]. The rail welding methods, which were developed on 1930-ies and are conventional at present time for railroads, decrease the problems with strikes, vibration and noise. However, heat effect during welding leads for forming of the heat-affected area (HAA) with usual hardness loss in it. Rail metal in the heat-affected area is more susceptible to wear and defects of contact-fatigue origination during operation. Several sources presented multiple examples of rail defects, leading to destruction and premature wear in a soft area of HAA of rail welded seams [6–8].

It is known that hardness loss in pearlitic rails is connected with areas of spheroidizing cementite [14–21], though genesis of thee structures usually is not discussed and is often considered as an evident consequence of welding heat supply. To understand such processes, we can examine the technical literature on phase transformations during processing of industrial steels, especially hypereutectoid steels (ball bearing and tool steels), which are well examined in the field of forming of their spheroidizing structures [17,18]. FBW process is

characterized as butt welding, when joining of components is achieved by heating via current resistance and consequent pressure applied to the contact surfaces of welding components [9–14]. Additionally, rail heating supports localized melting on the surfaces of rail joints. FBW process is divided by three stages.

Preliminary heating for decrease of mechanical resistance between contacting surfaces and decrease of upsetting force required for welding, is realized at the first stage. This heating promotes reducing of cooling rate after welding and preventing undesirable martensite transformation. The second stage (or so-called sparkling stage) is concluded in continuous rail motion with permanent speed and consequent motions of approximation and tearing-off. This stage includes forming of contact points on the surface of a rail joint owing to surface roughness. Strong electric current, which causes blinking, passes through these points. The third stage is presented by upsetting; compressing force is applied just after melting of a thin surface layer, so forging takes place between rails. At the final stage of upsetting, electric current is switched off automatically. To provide good welding quality, applied pressure should push out liquid metal, oxides and impurities out of separating surface, thereby providing metal-metal contact.

In the end of welding process, non-uniform temperature distribution along longitudinal cross section of the rail welded joint is observed [8–11]. The authors [10] noted that correct choice of welding parameters plays a decisive role in achievement of efficient desired combination of welded seam properties. However, there are several difficulties in control of a row of technological parameters for meeting the concrete requirements to connections with good level of tensile strength, destruction toughness and residual stresses. Additionally, high carbon content in the modern rail steels complicates welding due to increase of hardenability and possibility of $Fe_3C$ deposition on the boundaries of austenitic grains. Another critical moment is decrease of mechanical properties along the heat-affected area due to variation of eutectoid morphology, caused by non-uniform temperature distribution during welding. Eutectoid is not more pearlitic in the area of partial austenitization, while spheroidizing cementite has a structure of ferrite matrix; it leads to hardness loss and, consequently, to localized accelerated wear [14]. This research explained the mechanism of such spheroidizing as diluted eutectoid transformation (DET). According to [14–18], DET occurs in the conditions with presence of austenite inhomogeneities near the eutectoid plateau, when carbides remain non-soluble on austenite matrix. Austenite decomposition is accompanied by cooperative transformation ($\gamma \rightleftarrows \alpha + Fe_3C$ lamellar) in several areas, while in other areas non-cooperative eutectoid transformation occurs, with distribution of carbon atoms and spheroidizing of carbides by austenite/ferrite transformation front. In order to diminish these problems, the authors [20–23] showed that width decrease of spheroidizing area is an efficient method. However, decrease of spheroidizing area width leads to increase of extension stress in the rail joint area. The authors suggested several solutions, such as (1) heat treatment after welding via induction heating of a rail head and (2) lowering of heat supply (impulse current, number of impulses, time) at the stages of preliminary heating and melting, as well as increase of plastic deformation in longitudinal direction during upsetting.

The authors of the research [23] studied kinetics of isothermal phase transformations in rail steels and displayed that it is possible to obtain pearlitic microstructure for standard steel, which is refined in the same way as high-quality steels, at the same austenitization conditions. They suggested that it is caused due to building of a distinctly planned thermal profile after hot rolling of rails, taking into account the features of phase transformations in steel as a function of chemical composition. Another author [23] examined welding process and emphasized three various microstructural sections, which form a heat-affected area of a rail welded joint. He supposed that these areas present dangerous microstructural violations and are considered as preferential places of origination of fatigue cracks. Using the concept of phase transformation and the methodology based on dilatometry, he explained the cause of forming of these three various microstructural sections and proposed the alternative thermal welding cycle, which is based on controlled cooling after welding in order to decrease that microstructural heterogeneity.

Experimental evaluation of hardness distribution in a rail welded joint after welding cooling **is the aim of this research**.

## Materials and methods for research

Welding of rails was carried out in a spot-welding machine K-1000 (**Fig. 1**). Welding with continuous and pulsing melting was provided by uniform and high-concentrating heating of a rail joint during welding. Heat treatment was conducted in the induction heating furnace UIN-001-100/RT-S. According to the technological process at the enterprise, rail joint enters heat treatment procedure with residual temperature 350–450 °C. Measuring of metal temperature in a rail joint body is executed by electronic pyrometer. Operation was implemented with providing all required parameters. It is necessary to conduct additional joint heating at the residual temperature 250 °C during 30–80 s in manual mode, then to hold a pause 30 s and then to continue operation in automatic mode.

The experiments were carried out according to the following technique: after welding, accelerated cooling was conducted via three procedures.

1. Simple (natural) cooling after welding at 824 °C during 13–16 min and to 200 °C during 13–35 min.

2. Air spraying from 760 °C to 200 °C during 45 min.

3. Spraying with water–air mix from 760 °C to 200 °C during 40 min.

Technical parameters of a spot-welding machine K-1000: nominal voltage of electric power supply – 380 V; voltage of diesel generating power station – 80 V; nominal primary current (duty cycle 50 %) – 800 kVA; operating pressure in hydraulic system – 20 MPa; upsetting force – 800 KN (80,000 kgf); gripping force – 2,000 KN (200,000 kgf); mass – 8,800 kg; dimensions (width × height × length) – 1170 × 2475 ×3620 mm; welding time for rails R65 – 180 s.

**Fig. 1. Welded rail joint during processing in a spot-welding machine K-1000**

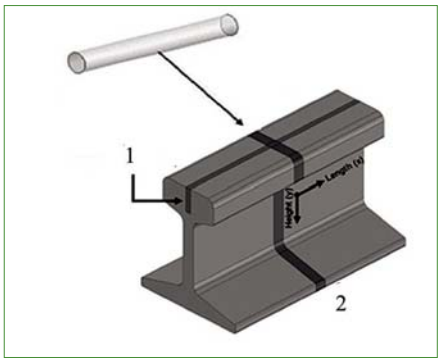


**Fig. 2. Scheme of shearing of samples for tensile testing:** 1 – center of rolling strip; 2 – welded joint

Then the samples for hardness measuring using stationary hardness testing gauge were sheared. Hardness was measured via Rockwell method on rolling surface of rail head (RSRH), with 4 mm interval and on the depth 10 and 22 mm.

Tensile testing of initial rail and rail which was welded according to the standard technology was carried out in the universal testing machine WDW-200E, meeting the requirements of the GOST 1497-84. Regulated values of parameters were taken from the clause 5.8 of the GOST R 51685-2013 for the rail of DT370IK category. Mechanical properties of rails during tensile testing were determined on cylinder samples (type III) at the room temperature. Semiproducts for these samples were sheared from a specimen head in the fillet area, close to rolling surface and along rolling direction (**Fig. 2**). 6 samples were fabricated for testing. Chemical composition was determined via X-ray spectral analysis according to the GOST 18895-97 by optical emission spectrometer Q4 Tasman. Regulating data of chemical elements for steel 90KhAF were taken from the clauses 5.4.1–5.4.3 of the GOST R 51685-2013. Testing on impact toughness determination was conducted in accordance with the GOST 9454-78 using impact pendulum machine IO 5003 0.3-11. Semiproducts for these samples were sheared from a specimen head in the fillet area, along rolling direction. Notch was applied on the samples from the side of rolling surface of a rail head. 3 samples from a standard rail, which was subjected to butt welding, were fabricated for testing. Geometrical parameters of notch were controlled using universal measuring microscope UIM-23.

To reveal the structure of rail steel samples, pickling of micro-polished sections was conducted in 3 % solution of nitric acid. Microstructure was examined using microscope MikroMet2, digital microscope Olympus GX41A with magnification ×50, ×100, ×200, ×500 and ×1000. Electron microscope examinations were carried out using electron microscope LV-4501 JEOL equipped with energy dispersion spectrometer. The system of signal processing separates X-ray photons by energies and thereby we obtain a complete spectrum for consideration on elementary composition in a target sample.

## Results of the research

The results of tensile testing of the samples (average data for 3 samples from each series) are presented in the **Table 1**. Chemical composition is presented in the **Table 2**. The main metal meets the requirements of the GOST 51685-2013. However, average decrease of yield strength by 8 % and tensile strength by 15 % were observed for welded joints, and it was accompanied by small increase of elongation. Lowering of material yield strength and tensile strength as a result of welding can be explained by structural variations (which were mention in introduction), such as partial cementite globalization on pearlite and increase of interlamellar spacing. Vanadium content in the samples of railroad rails R65 IK of steel 90KhAF, which were presented for testing and determination of chemical composition, was 0.077 and 0.079 %, while regulating data are within the range 0.08–0.15 %. Carbon content in the welded rail decreased by 6 % (regulating data is 0.83–0.95 %).

Microstructural characteristics of welding joints are presented by five various areas: axial line of welded joint, grain growth, grain comminution, partial austenitization (spheroidized $Fe_3C$ or diluted eutectoid) and basic metal. The main microstructures of welded joint along the melting line and of the heat-affected area are shown on the **Fig. 3**. Butt welding with melting includes seven separated areas, which are symmetric in relation to the center.

Forming of thin pearlitic and hypoeutectoid ferritic grains is observed along the medium line of a rail welded seam (**Fig. 3, *a***). Forming of hypoeutectoid ferrite occurs due to high temperature, which is reached during welding, decarburizing layer is created as a result. Decarburization is a usual appearance during FBW process, it has usually no effect on mechanical properties of welded joint. It can be noted that mixed ferritic-pearlitic structure is formed in the area of a melting line. Microstructure in the area of complete austenitization is presented by lamellar pearlite (**Fig. 3, *b***), ferrite was not revealed.

In the area of partial austenitization of rails, forming of diluted eutectoid is observed. $Fe_3C$ particles in this area look like spheres, deposited in ferritic matrix and existing together with several small pearlite colonies (**Fig. 3, *c***).

The results of hardness measuring after welding are presented in the **Fig. 4** and **Fig. 5**, which are coincided with macro-picture of transversal template of a welded joint.

The results of testing on determination of impact toughness (average data for 3 samples from each series) are presented in the **Table 3**. Metal defects in sample fractures after impact testing were not revealed.

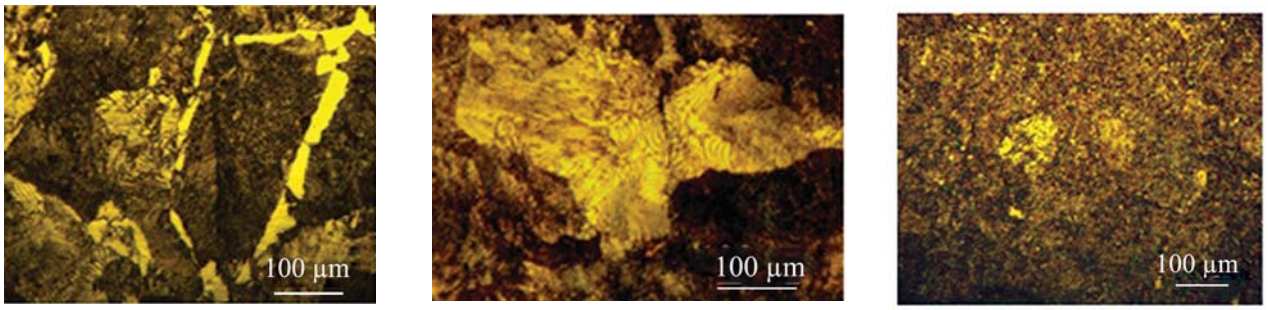


*a* *b* *c*

**Fig. 3. Microstructure of welded seam:** *a* – along melting line; *b* – in the area of complete austenitization; *c* – in the area of partial austenitization

Table 1. The results of tensile testing

| No. of sample | Testing results | | | |
|---|---|---|---|---|
| | Tensile strength, N/mm² | Yield strength, N/mm² | Relative elongation, % | Relative reduction of area, % |
| Welded rail | 1060 | 805 | 12 | 54 |
| Standard rail | 1260 | 870 | 12 | 36 |

Table 2. The results of testing for chemical composition determination

| Chemical element | Regulating data value, GOST R 51685-2013, % | Actual value, % | | | |
|---|---|---|---|---|---|
| | | Variation 1 | Variation 2 | Variation 3 | Average |
| The sample of initial rail | | | | | |
| Carbon | 0.83–0.95 | 0.860 | 0.864 | 0.852 | 0.859 |
| Manganese | 0.75–1.25 | 0.818 | 0.831 | 0.822 | 0.824 |
| Silicon | 0.25–0.60 | 0.535 | 0.535 | 0.527 | 0.532 |
| Vanadium | 0.08–0.15 | 0.077 | 0.077 | 0.076 | 0.077 |
| Chromium | 0.20–0.60 | 0.423 | 0.425 | 0.417 | 0.422 |
| Phosphorus, not more | 0.020 | 0.009 | 0.010 | 0.008 | 0.009 |
| Sulfur, not more | 0.020 | 0.006 | 0.007 | 0.005 | 0.006 |
| Aluminium, not more | 0.004 | 0.002 | 0.001 | 0.002 | 0.002 |
| Copper, not more | 0.20 | 0.129 | 0.132 | 0.129 | 0.130 |
| Nickel, not more | 0.15 | 0.084 | 0.085 | 0.084 | 0.084 |
| Nickel+ copper, not more | 0.27 | 0.213 | 0.217 | 0.213 | 0.214 |
| Titanium, not more | 0.010 | 0.003 | 0.003 | 0.003 | 0.003 |
| Nitrogen | 0.010–0.020 | 0.010–0.020 | 0.010–0.020 | 0.010–0.020 | 0.010–0.020 |
| The sample in the area of welded joint | | | | | |
| Carbon | 0.83–0.95 | 0.808 | 0.812 | 0.801 | 0.807 |
| Manganese | 0.75–1.25 | 0.830 | 0.836 | 0.830 | 0.832 |
| Silicon | 0.25–0.60 | 0.532 | 0.534 | 0.548 | 0.538 |
| Vanadium | 0.08–0.15 | 0.078 | 0.078 | 0.081 | 0.079 |
| Chromium | 0.20–0.60 | 0.426 | 0.423 | 0.423 | 0.424 |
| Phosphorus, not more | 0.020 | 0.011 | 0.010 | 0.11 | 0.011 |
| Sulfur, not more | 0.020 | 0.008 | 0.007 | 0.007 | 0.007 |
| Aluminium, not more | 0.004 | 0.001 | 0.001 | 0.002 | 0.001 |
| Copper, not more | 0.20 | 0.130 | 0.134 | 0.135 | 0.133 |
| Nickel, not more | 0.15 | 0.084 | 0.087 | 0.088 | 0.086 |
| Nickel+ copper, not more | 0.27 | 0.214 | 0.221 | 0.223 | 0.219 |
| Titanium, not more | 0.010 | 0.003 | 0.003 | 0.004 | 0.003 |
| Nitrogen | 0.010–0.020 | 0.010–0.020 | 0.010–0.020 | 0.010–0.020 | 0.010–0.020 |

Table 3. The results of testing on determination of impact toughness

| No. of the sample | Regulating value, J/cm² | Kind of testing | Side $H_1$, mm | Side B, mm | Cross section square, cm² | Work, J | Impact toughness, J/cm² |
|---|---|---|---|---|---|---|---|
| Standard rail | 15, not less | KCU | 8.05 | 9.98 | 0.803 | 9.0 | 21 |
| Welded rail joint | | | 8.09 | 9.98 | 0.807 | 9.5 | 19 |

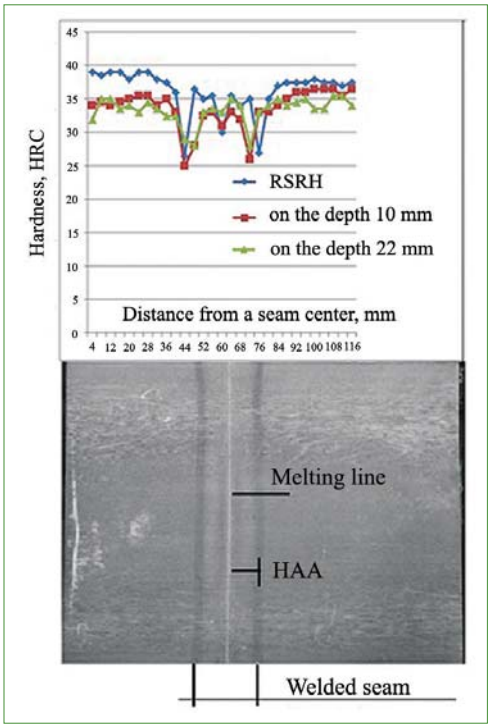


**Fig. 4. Macrostructure of welding seam, coincided with hardness distribution**

The central distinct line marks the place of rails joining and the place, where melting occurred during welding. High temperatures and oxidizing atmosphere lead to moderate decarburization of this area. That's why this line displays another behaviour in pickling and lower hardness (presented due to pro-eutectoid ferrite). Other areas are symmetric in relation to the central line. Dropping of hardness is fixed in the area of partial austenitization of rails. Consequent heat treatment (quenching) of welded joint does not correct this disadvantage, but only increases the heat-affected area with varied structure by 1.5–2.0 times. Width of the welded joint is 40–46 mm after welding and 140 mm after heat treatment.

Experimental results of accelerated cooling after welding within the temperature range from 760 to 200 °C are presented in the **Fig. 6** and **Fig. 7**. It can be seen that hardness dropping in the area of partial austenitization of a welded joint was minimized successfully. Hardness parameters correspond to pearlitic structure of the main rail metal. Use of the cooling procedure with water-air mix leads to increase of hardness on rolling strip of a rail head (RSRH) to 45–58 units, what testifies on forming of martensite and bainite structures. At the same time, these transformation were not observed on the depths 10 and 22 mm, and hardness is on the level of pearlitic structure of the main rail metal.

## Discussion of the results

Analysis of the values of mechanical properties after testing, we can see decrease of the yield strength and tensile strength of materials as a result of butt welding with melting: it can be explained by structural variations, such as partial cementite globalization in pearlite and increase of interlamellar distance [17, 23–26].

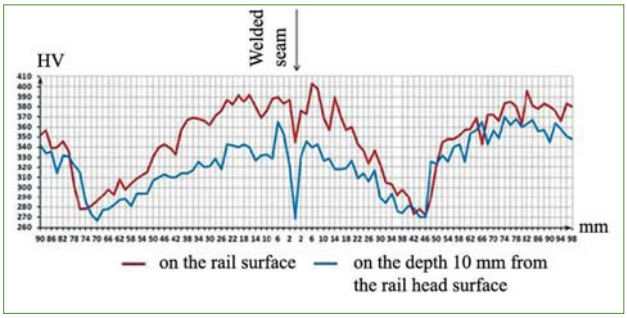


**Fig. 5. Hardness distribution in a welded joint after conventional heat treatment**

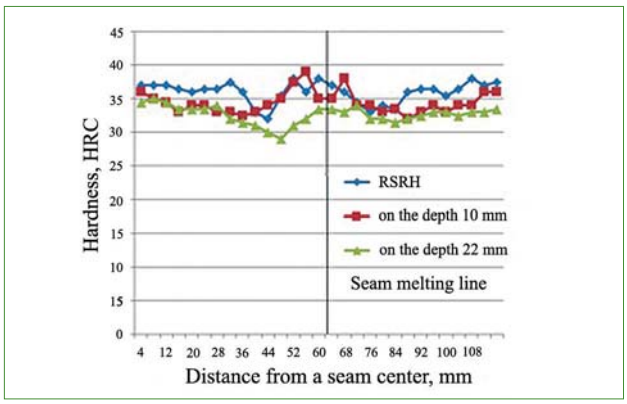


**Fig. 6. Hardness distribution for sprayer use only with air**

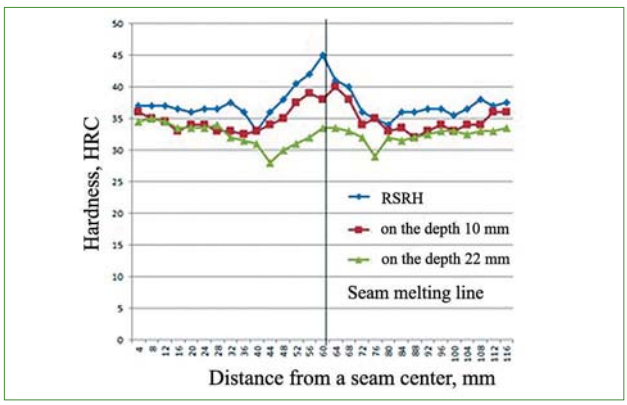


**Fig. 7. Hardness distribution for sprayer use with water-air mix**

The authors [23, 24] displayed that partial pearlite spheroidizing by cementite increased wearing rate and varies plastic flow on rail surface. To substantiate forming of proto-eutectoid $Fe_3C$ on the boundaries of grains, the authors of another researches [15, 23] suggested two hypotheses. Firstly, cooling rate using in production of rails was insufficient for depression of forming of proto-eutectoid $Fe_3C$, or, secondly, addition of alloying elements was insufficient for reaction with carbon excess, what promotes nuclei origination and growth of $Fe_3C$ particles before the eutectoid reaction. It is important to be noted, that the temperatures during welding are higher in the center along the melting line and lower apart from it. However, spheroidizing rises quickly after minimal hardness values (and maximal spheroidizing) and then dramatically falls with increase of distance from the center (what can be seen also by hardness behaviour).

This process is incompatible with the classical spheroidizing mechanism, but it id compatible with diluted eutectoid transformation (DET) [15–17], when spheroidizing occurs in the area with lower austenitization, but above the temperature $A_{c1}$, because there is more amount of carbide nuclei in a sample during cooling. Spheroidizing falls dramatically down to zero, when the reached temperature is below $A_{c1}$ value. However, partial spheroidizing takes place at higher temperatures, because carbide-free areas transform in a classical eutectoid. Large difference in grain size in the end of this area can be considered as transition between the main metal and the heat-affected area, which creates a separating boundary with the maximal temperature equal to $A_{c1}$. In other words, the minimal rail temperature far from this line does not reach the temperature $A_{c1}$, while on the other side of this line (the heat-affected area, close to the central line) the maximal temperature is above $A_{c1}$ value and austenitization consequently takes place. However, austenitization is not complete in the spheroidizing area, and grain growth can't occur.

Thermodynamic simulation for these steels shows 3-phase eutectoid area and intercritical area with equilibrium between austenite and cementite [23, 25–32], what testifies on eutectoid feature of the material for this composition and favors diluted eutectoid transformation. The temperatures of eutectoid gap are close for all rails and they are well predicted by calculations; however, predicted temperatures $A_{cm}$ are rather lower than actual temperatures $A_{cm}$, which are monitored using dilatometry. It was expected, because calculation show thermodynamic equilibrium, which is far from the obtained situation with permanent heating of samples (even at the low heating rates). This difference is large owing to low kinetics of cementite dissolution, especially if it contains alloying elements (such as chromium and manganese) [1–3, 21–23]. After-welding treatment simulated successfully the spheroidizing area in a welded rail. Maximal spheroidizing was achieved for a conventionally welded rail without accelerated cooling. The rail sample, which was subjected to accelerated cooling from 760 °C after welding, contains mainly lamellar cementite.

In conclusion we note technological consequences of this research. It seems to be evident, that DET in pearlitic structures is inevitable sequence of the temperature gradient, which is created by welding. However, it is known, that several variables influence on its forming and minimize it. It was suggested [17, 18], that alloying elements can avoid hardness loss, but at the same time these elements will probably retard dissolution of carbides (because this loss occurs as a result of diluted eutectoid transformation) [15] and, respectively, they can expand the area of hardness loss in a welded seam HAA. Accelerated cooling in this area after welding, which can support classical eutectoid (not diluted one) is considered as another possible solution. But such approach is criticized by producers, because it can lead (on their opinion) to martensite forming. It is also necessary to keep a technological interval: it is prohibited to set welding parameters in such way, that welded seam will be cooled too slowly (less than 1 °C/s) or too quickly (more than 10 °C/s) [7, 8, 11–13], what can lead to martensite transformation. The authors think that it is required to continue the research in this direction, what is planned to realize in the following investigations. At present time, several companies use additional heat treatment of welded seams in order to restore hardness in this area, but it is an additional process with excessive expenses, which can be avoided via introduction of controlled cooling in the end of welding process. The obtained results, which are presented in this work, show incorrectness of such processing of a welded seam, when hardness loss is not eliminated. The authors declare their readiness to open discussion about this problem and conduction of joint researches.

## Conclusions

1. Butt welding with melting presented seven separated areas, which are symmetric relating to the center, with pearlitic-ferritic microstructure on connection line; then microstructure varies to completely pearlitic, completely spheroidized and again completely pearlitic in direction of motion to the main metal. Pearlitic areas were characterized by usual hardness and behaviour during pickling, while the spheroidized area demonstrated another behaviour during pickling and lower hardness (both dramatically varying in direction of motion to the main metal and gradually to the center). The welding parameters played an important role in increase or decrease of width of the partial austenitization area.

2. Possibility of decrease of pearlite spheroidizing due to accelerated cooling within the temperature range from 760 to 200 °C is displayed experimentally. It is shown that the part of lamellar cementite in the area of incomplete austenitization rises with increase of the cooling rate. It leads to hardness increase in the area of welded seam.

## REFERENCES


1. Smirnov L. A. et al. quality improvement of railroad rails. *Chernaya metallurgiya. Byulleten naucho-tekhnicheskoy i ekonomicheskoy informatsii.* 2005. No. 6. pp. 43–49.
2. Shur E. A. Damages of rails. Moscow : Intekst. 2012. 192 p.
3. Schastlivtsev V. M., Yakovleva I. Ya. Thin-lamellar pearlite – the first volumetric nano-material in carbon steel. *Izvestiya RAN. Seriya fizicheskaya.* 2015. Vol. 79. No. 9. pp. 1221–1224.
4. Prospective directions of the rail industry development. Technologies of production and operation. *Materials of the V International scientific-technical conference. Sochi. May 24–25, 2022.* Moscow : OOO «EVRAZ». 2023. 228 p.
5. Alekhin A. L., Alekhin L. I. On metal hardness in welded joints and roughness on rail rolling surfaces. *Put i putevoe khozyaistvo.* 2013. No. 11. pp. 9–10.
6. Gromov V. E., Yuryev A. B., Morozov K. V., Ivanov Yu. F. Microstructure of quenched rails. Novokuznetsk : Inter-Kuzbass. 2014. 216 p.
7. Shtaiger M. G., Balanovskiy A. E. Analysis of welding technologies for high-strength rails from the position of structure forming in building and reconstruction of high-speed railroads. Part 1. *iPolytech Journal.* 2018. Vol. 22 (6). pp. 48–74.
8. Shtaiger M. G., Balanovskiy A. E. Analysis of welding technologies for high-strength rails from the position of structure forming in building and reconstruction of high-speed railroads. Part 2. *iPolytech Journal.* 2018. Vol. 22 (7). pp. 41–68. DOI: 10.21285/1814-3520-2018-7-41-68.
9. Genkin I. Z. Welded rails and turnout switches. Moscow : Intekst. 2003. 93 p.

10. Dotsenko V. E. Contact welding of rails. Moscow : Mashgiz. 1949. 312 p.
11. Kuchuk-Yatsenko S. I., Khryashcheva N. K., Shlyapin V. B. The process of continuous melting during contact welding. *Put i putevoe khozyaistvo*. 1973. No. 1. pp. 9–10.
12. Kuchuk-Yatsenko S. I., Krivenko V. G., Bogorskiy M. V. Intensification of rail heating during contact welding with impulse melting. *Avtomaticheskaya svarka*. 1977. No. 4. pp. 45–50.
13. Kuchuk-Yatsenko S. I. Contact butt welding with continuous melting. Kiev : Naukova dumka. 1976. 213 p.
14. Bauri L. F. et al. The role of welding parameters on the control of the microstructure and mechanical properties of rails welded using FBW. *Journal of Materials Research and Technology*. 2020. Vol. 9. No. 4. pp. 8058–8073.
15. 15. Verhoeven J. D., Gibson E. D. The divorced eutectoid transformation in steel. *Metallurgical and Materials Transactions A*. 1998. Vol. 29. pp. 1181–1189.
16. Nishikawa L. P., Goldenstein H. Divorced Eutectoid on Heat-Affected Zone of Welded Pearlitic Rails. *JOM*. 2019. Vol. 71. pp. 815–823. DOI: 10.1007/s11837-018-3213-5.
17. Schastlivtsev V. M., Mirzaev D. A., Yakovleva I. L. et al. Pearlite on carbon steels. Ekaterinburg: UrO RAN. 2006. 312 p.
18. Tushinskiy L. I., Bataev A. A., Tikhomirova L. B. Pearlite structure and steel constructive strength. Novosibirsk: Nauka. 1993. 280 p.
19. Bauri L. F., Alves L. H. D., Pereira H. B., Tschiptschin A. P., Goldenstein H. The role of welding parameters on the control of the microstructure and mechanical properties of rails welded using FBW. *Journal of Materials Research and Technology*. 2020. Vol. 9. No. 4. pp. 8058–8073.
20. Rodrigues K. F., Mourão G. M. M., Faria G. L. F. Kinetics of isothermal phase transformations in premium and standard rail steels. *Steel Res. Int*. 2021. Vol. 92. No. 1. 2000306. DOI:10.1002/srin.202000306.
21. Porcaro R. R., Faria G. L., Godefroid L. B., Apolonio G. R., Candido L. C., Pinto E. S. Microstructure and mechanical properties of a flash buttwelded pearlitic rail. *Journal of Materials Processing Technology*. 2019. Vol. 270. pp. 20–27.
22. Godefroid L. B., Moreira L. P., Vilela T. C. G., Faria G. L., Candido L. C., Pinto E. S. Effect of chemical composition and microstructure on the fatigue crack growth resistance of pearlitic steels for railroad application. *Int. J. Fatigue*. 2019. Vol. 120. pp. 241–53.
23. Porcaro R. R. et al. Microstructure and mechanical properties of a flash butt welded pearlitic rail. *Journal of Materials Processing Technology*. 2019. Vol. 270. pp. 20–27.
24. Offerman S. E., van Wilderen L. J. G. W., van Dijk N. H., Sietsma J., Rekveldt M. T., van der Zwaag S. In-situ study of pearlite nucleation and growth during isothermal austenite decomposition in nearly eutectoid steel. *Acta Mater*. 2003. Vol. 51. No. 13. pp. 3927–38.
25. García de Andrés C., Caballero F. G., Capdevila C., Álvarez L. F. Application of dilatometric analysis to the study of solid-solid phase transformations in steels. *Mater Charact*. 2002. Vol. 48. No. 1. pp. 101–11.
26. Marder A. R., Bramfitt B. L. The effect of morphology on the strength of pearlite. *Metall Trans. A, Phys. Metall Mater. Sci*. 1976. Vol. 7 (3). pp. 365–372.
27. Hyzak J. M., Bernstein I. M. The role of microstructure on the strength and toughness of fully pearlitic steels. *Metall Trans. A, Phys. Metall Mater. Sci*. 1976. Vol. 7 (8). pp. 1217–1224.
28. Tressia G., Sinatora A., Goldenstein H., Masoumi M. Improvement in the wear resistance of a hypereutectoid rail via heat treatment. *Wear*. 2020. No. 442–443. 203122.
29. Cezário A. L. S., Porcaro R. R., Faria G. L. Proposition of an empirical model for determination of critical temperatures during continuous cooling in heat affected zones of IF steels welded by the TIG Process. *Soldag Insp*. 2019. Vol. 24. pp. 1–14.
30. Balanovskiy A. E., Shtaiger M. G., Kondratyev V. V., Karlina A. I. Determination of rail steel structural elements via the method of atomic force microscopy. *CIS Iron and Steel Review*. 2022. Vol. 23. pp. 86–91.
31. Rezanov V. A., Martyushev N. V., Kukartsev V. V., Tynchenko V. S., Kukartsev V. A., Grinek A. V., Skiba V. Yu., Lyosin A. V., Karlina A. I. Study of melting methods by electric resistance welding of rails. *Metals*. 2022. Vol. 12. No. 12. p. 2135.
32. Elemessov K., Baskanbayeva D., Martyushev N. V., Skeeba V. Y., Gozbenko V. E., Karlina A. I. Change in the properties of rail steels during operation and reutilization of rails. *Metals*. 2023. Vol. 13. No. 6. p. 1043.